Simulation of rapid sand filters to understand and design sequential iron and manganese removal using reactive transport modelling

Kruisdijk, Emiel; van Breukelen, Boris M.; van Halem, Doris

DOI
10.1016/j.watres.2024.122517

Publication date
2024

Document Version
Final published version

Published in
Water Research

Water Research 267 (2024) 122517

Contents lists available at ScienceDirect

Water Research

journal homepage: www.elsevier.com/locate/watres

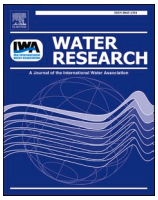

Simulation of rapid sand filters to understand and design sequential iron and manganese removal using reactive transport modelling

Emiel Kruisdijk *, Boris M. van Breukelen, Doris van Halem

Delft University of Technology, Faculty of Civil Engineering and Geosciences, Department of Water Management, Stevinweg 1, 2628 CN Delft, the Netherlands

ARTICLE INFO

Keywords:
Reactive transport modelling
PHREEQC
rapid sand filters
Oxidation
PEST
Iron

ABSTRACT

Iron (Fe^{2+}), manganese (Mn^{2+}), and ammonium (NH_4^+) oxidation processes were studied in three single media and three dual media full-scale rapid sand filters (RSFs) using reactive transport modelling (RTM) in PHREEQC and parameter estimation using PEST. Here, we present the insights gained into the spatial distribution of Fe and Mn mineral coatings in RSFs and its influence on the oxidation sequence and rates. Fe^{2+} and Mn^{2+} oxidation predominantly occurred simultaneously in the RSFs, contrary to the expected sequential oxidation based on Gibbs free energy calculations. During backwashing, RSF grains become fully mixed, which initiates heterogeneous Mn^{2+} oxidation on Mn-coated grains that end up in the top layer. The resulting grains have a mixed Fe/Mn mineral coating, which is limiting heterogeneous Mn^{2+} oxidation due to the limited Mn mineral surface available. Mixed coatings did not seem to affect Fe^{2+} oxidation rates, instead oxidation rates were increasing at lower pH. We found that RSFs can be designed to spatially separate Fe^{2+} and Mn^{2+} oxidation, which results in optimal conditions for Mn^{2+} oxidation. The RSF needs to consist of two layers with varying density to inhibit mixing and complete Fe^{2+} oxidation should occur in the top layer. The developed RTM can be used to estimate the depth at which Fe^{2+} oxidation is complete, and thus the ideal intersection depth of the two layers. A novel perspective is provided on how mineral coating distribution in single and dual media filters influence removal rates and the sequence of oxidation, which contributes to the design of more efficient groundwater filters.

1. Introduction

Groundwater provides drinking water to at least half the global population (Connor, 2015). Anaerobic groundwaters generally contain dissolved iron (Fe^{2+}), manganese (Mn^{2+}), and ammonium (NH_4^+) concentrations exceeding drinking water standards. Rapid sand filters (RSFs) are designed to remove these solutes after aeration or oxidant dosing (e.g., $KMnO_4$, Cl_2). If these constituents are not removed properly, they will; (i) negatively affect human health, (ii) clog the distribution system, (iii) create stains during laundry, and/or (iv) affect colour, taste, and odour of drinking water (Tekerlekopoulou et al., 2013). In RSFs, removal occurs by a combination of physicochemical and biological processes in the supernatant water as well as during transport through the filter media (Freitas et al., 2022). They are effective, nature-based, easy to use, relatively low-cost and consume low energy and chemicals. Therefore, RSFs are commonly used in e.g., Western Europe, the United States of America, and Canada, and could also play a major role in areas that do not yet have access to safe potable water in accordance with United Nations' Sustainable Development Goal 6.

Aeration of the anaerobic groundwater before filtration initiates redox processes responsible for most of the removal of Fe^{2+}, Mn^{2+}, and NH_4^+. Fe^{2+} and Mn^{2+} oxidation can occur via three different reaction pathways: chemical homogeneous (or flocculent) oxidation, chemical heterogeneous (or adsorptive, autocatalytic, or contact) oxidation, and biological heterogeneous oxidation (Davies and Morgan, 1989; Kappler et al., 2021; Tebo et al., 2005). The formed Fe^{3+} and Mn^{4+} hydrolyse and precipitate as poorly soluble amorphous metal-(hydr)oxides and are, consequently, removed from the water phase. Fe^{2+} oxidation can take place in RSF via all three pathways. RSF are periodically backwashed to remove Fe precipitates, as these start clogging the top of the filter bed after treating a certain volume of groundwater. Dual media filters have a top layer of anthracite or pumice, and a bottom layer of sand. Bed resistance builds up slower in the anthracite layer due to the higher porosity and consequent larger storage capacity for precipitates resulting in longer runtimes compared to single media sand filters (Zouboulis et al., 2007).

Contrarily to Fe^{2+} oxidation, homogeneous Mn^{2+} oxidation is not

* Corresponding author.
E-mail address: e.kruisdijk@tudelft.nl (E. Kruisdijk).

https://doi.org/10.1016/j.watres.2024.122517
Received 26 June 2024; Received in revised form 19 September 2024; Accepted 23 September 2024
Available online 24 September 2024

expected in RSFs, as half times are in the order of years compared to residence times in the order of tens of minutes in RSFs (Diem and Stumm, 1984). Heterogeneous Mn^{2+} oxidation can be orders of magnitude faster, but is largely controlled by the amount of Mn-(hydr) oxides available to catalyse the process (Stumm et al., 1996). Nitrification is solely a biological process, which is conducted by autotrophic bacteria (Lee et al., 2014). NH_4^+ is transformed by a two-step reaction, where first nitrite is formed, and subsequently nitrate, by ammonium-oxidizing and nitrite-oxidizing bacteria, respectively, or by bacteria capable of complete nitrification (so-called commamox bacteria) (van Kessel et al., 2015).

These redox reactions have been extensively studied in previous research, and specific rate equations have been reported for most abiotic reactions (homogeneous Fe^{2+} oxidation: Sung and Morgan (1980); chemical heterogeneous Fe^{2+} oxidation: Tamura (1976); homogeneous and heterogeneous Mn-oxidation: Davies and Morgan (1989)). However, rate constants are often not available for heterogeneous oxidation under the specific conditions in RSF, as they are influenced by, for example, mineral structure, morphology, and reactive surface area of the grain coatings (Beckingham et al., 2016; Sung and Morgan, 1980). Similarly, rate constants of biological oxidation processes can vary substantially, as they are dependent on, for example, the abundances of oxidizing bacteria and their activity (Greskowiak et al., 2017; Kappler et al., 2021). RSF are such complex systems, because physical, microbiological, and chemical processes are coupled and occur simultaneously in a timespan of minutes. Therefore, multi-component geochemical reactive transport models (RTM) are essential to unravel these coupled processes, and can be applied to test the possibility of various reaction networks, reaction rates, and factors that control these rates (Kruisdijk and van Breukelen, 2021; Siade et al., 2021; Steefel et al., 2005).

Based on the theory of Gibbs free energy, Fe^{2+} oxidation (potential (E): +0.77 V) is more favourable at pH=7 with 1 M concentrations, than Mn^{2+} oxidation (+0.40 V) and will therefore occur first (Appelo and Postma, 2004). This difference will be further exaggerated by the often higher concentrations of Fe^{2+} in abstracted groundwater compared to Mn^{2+}. Hence theoretically, this oxidation sequence should result in Fe-coated sand in the top layer of the filter and Mn-coated sand at the bottom layer (Fig. 1A). However, in practice Fe- and Mn-coated sand grains will be mixed in single media filters during backwashing (Fig. 1B). The Mn-oxide coating in the top of the filter will catalyse oxidation and initiate heterogeneous Mn^{2+} oxidation. This results in relevant oxidation of Mn^{2+} in the top layer. This mixing does not occur in dual media filters, as the grains in the two layers do not mix due to the variation in size and density (Fig. 1C). This affects the sequence of oxidation, as oxidation of Fe and Mn occurs simultaneously in a single media filter (Gude et al., 2016), while oxidation is sequential in some dual media filters (Corbera-Rubio et al., 2023; Haukelidsaeter et al., 2023). In the current study, we developed a RTM simulating Fe^{2+}, Mn^{2+}, and NH_4^+ oxidation processes with the aim, (i) to assess the variations in oxidation kinetics observed with depth at three single and three dual media RSFs in the Netherlands, and (ii) to use obtained insights to understand sequential oxidation in RSFs and enable its design. The insights gained from the RTM provide a novel perspective on how mineral coating distribution in single and dual media filters influence removal rates and the sequence of oxidation, which provides insights for the design of more efficient groundwater filters.

2. Methods

2.1. Sampling and analysis

The RSFs studied are all situated in drinking water treatment plants in the Netherlands. Their function is to treat groundwater for drinking water purposes based on aeration and filtration. The single media RSF beds (RSF-S1, RSF-S2, and RSF-S3) are solely composed of quartz sand grains. The dual media RSFs beds (RSF-D1, RSF-D3, and RSF-D2) are build-up by a top layer of anthracite and a bottom layer of quartz sand.

Filtered water samples (0.45 μm) were taken from the supernatant and at several depths in the filter bed and stored at 4 °C before analysis. These samples were acidified (ROTIPURAN® Ultra 69%, 1% v/v) and analysed for Fe^{2+}, Mn^{2+}, SO_4^{3-}, Ca^{2+}, Mg^{2+}, PO_4^{3-}, and Si using

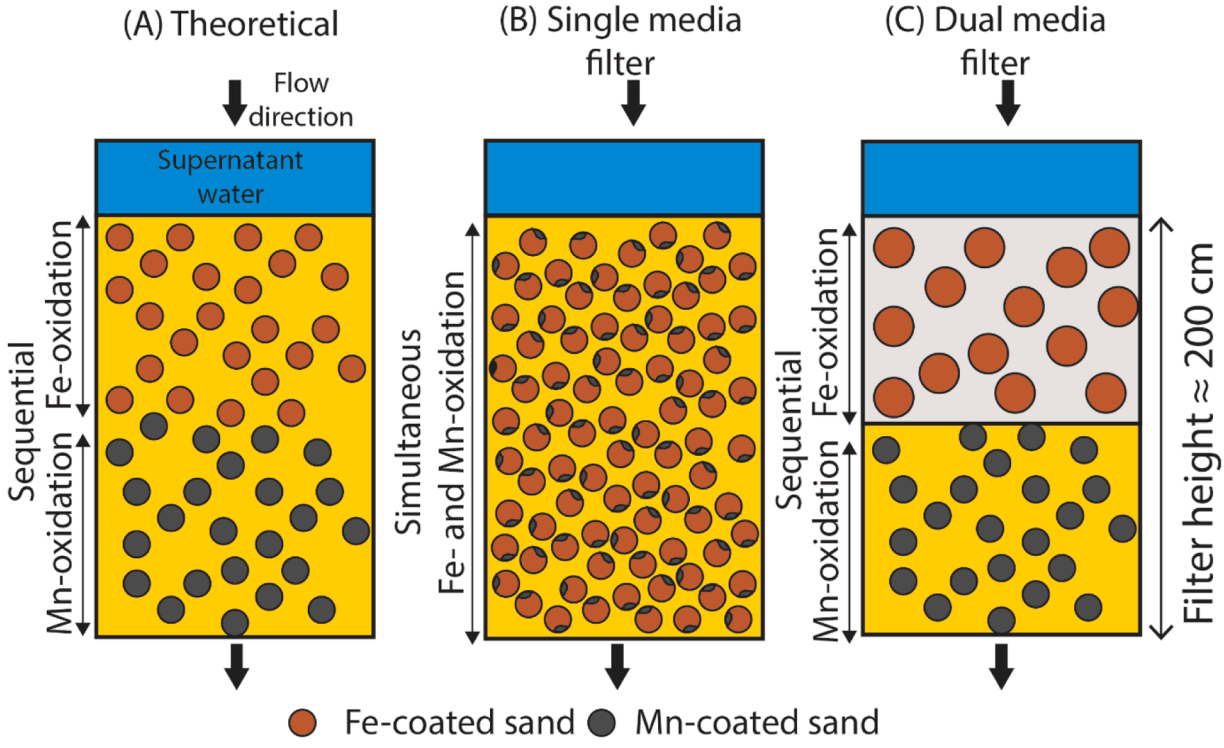

Fig. 1. Sequence of oxidation and distribution of Fe- and Mn-coated sand in theory (A), and in single and dual media sand filters (B and C, respectively).

inductively coupled plasma mass spectrometry or inductively coupled plasma optical emission spectroscopy. Discrete analysis or ion chromatography was performed to analyse alkalinity, NH_4^+, and NO_3^-, while temperature, pH, and O_2 was measured using sensors directly on-site. Furthermore, grain coatings were analysed using light microscopy (VHX-5000 series, Keyence).

2.2. Rapid sand filters characteristics and influent water quality

Table 1 provides an overview of the operational conditions and the dimensions of the six studied full-scale RSFs, as well as their influent water compositions. For all RSFs, supernatant levels were approximately 0.4 m, except for RSF-S3 where the supernatant level was 0.2 m. Filter media age ranged from 0.25 to >22 years.

Influent pH ranged from 6.9 for RSF-S3 and RSF-D3 to 8.0 for RSF-D2. Relatively high Fe^{2+} concentrations were observed in the influent water of RSF-S3 and RSF-D1 (±28 mg/L), while lower Fe^{2+} concentrations were measured in the other RSFs (range 1.2–6.0 mg/L). Similarly, NH_4^+ concentrations were also highest at RSF-S3 and RSF-D1 (±2.3 mg-N/L), while substantially lower at the other RSFs (ranging from 0.27–0.45 mg-N/L). Mn^{2+} concentrations were relatively low at RSF-S1 (0.035 mg/L), and ranged from 0.2–0.9 mg/L at the remaining RSFs. O_2 concentrations were close to saturation at RSF-S1, RSF-S2, and RSF-D1 (ranging from 9.2–10.0 mg/L), and slightly undersaturated at RSF-S3, RSF-D2, and RSF-D3 (4.6–6.5 mg/L).

2.3. Conceptual model

The model was developed in PHREEQC: a regularly applied open access multi-component geochemical 1-D reactive transport model often used to simulate coupled processes, for example to study water quality effects of managed aquifer recharge (Antoniou et al., 2013), surface complexation processes in groundwater (Appelo et al., 2002), and nutrient fate in aquifers (Kruisdijk and van Breukelen, 2021). PHREEQC enables studying interactions between different equilibrium and kinetic reactions, and their influences on, for example, alkalinity, pH, and O_2 concentration profiles. The PHREEQC 3.0 plugin for Notepad++ was used to write, edit, and run the input files (Parkhurst and Appelo, 2013). The WATEQ4F database was used and provided the equilibrium constants for thermodynamic reactions. The database was modified to kinetically simulate the oxidation of Fe^{2+}, NH_4^+, and Mn^{2+}. The valence states of these solutes were decoupled from the database, following, for example, Antoniou et al. (2013) and Rahman et al. (2015).

We departed from the conceptual model of Vries et al. (2017), but our model and its application deviates on three points. First, nitrification was simulated in our model, which enabled making a redox mass balance comparing reductants to oxidants. Nitrification influences the O_2 concentrations and pH in the water-phase and therefore also impacts Fe^{2+} and Mn^{2+} oxidation rates (Lee et al., 2014; Tatari et al., 2013). Second, PEST (Doherty, 1994) was used to estimate unknown parameters in the rate equations to get a best fit between observed and simulated concentration profiles. Third, the model outcomes of the six RSFs and the estimated rate constants were used to compare the functioning of the RSFs.

Fig. 2 displays the conceptual reaction network of the simulated coupled processes. The model is divided in two sub-models. The first sub-model simulates the redox processes in the supernatant water, which are initiated by the aeration of groundwater before it is discharged on top of the supernatant layer (see further section 2.4). The resulting water composition of the supernatant simulation was used as input composition for the second part: the filter bed simulation, where the biogeochemical processes are simulated in the filter bed (details in section 2.5). For each RSF, a separate model was set up consisting of a supernatant and a filter bed simulation.

2.4. Supernatant simulation

Biogeochemical processes in the supernatant were simulated in a

Table 1
Overview of operational parameters and design characteristics of the rapid sand filters (RSFs), and the aerated influent water composition.

Location	RSF-S1	RSF-S2	RSF-S3	RSF-D1	RSF-D2	RSF-D3
Operational parameters and design characteristics						
Filter bed	Single	Single	Single	Dual	Dual	Dual
Flow velocity (m/hr)	4.8	5	10	5	6.6	5.7
Bed height (m) total	2.17	2.00	2.10	2.10	2.00	2.60
Anthracite layer (m)	0	0	0	1.00	1.00	0.60
Sand layer (m)	2.17	2.00	2.10	1.00	1.00	2.00
Filter media age (years)	19	>22	0.6	0.25	8	Anthracite: 1 Sand: 5
Supernatant water level (m)	0.4	0.4	0.2	0.4	0.4	0.4
Aerated influent water composition						
Temperature (°C)	12	11	11	11	11	12
pH (-)	7.9	7.6	6.9	7.2	8	6.9
DOC (mg/L)	2.2	1.5	n.m.	n.m.	2.6	n.m.
O_2 (mg/L)	10	9.2	4.6	9.6	6.5	5.8
NH_4^+-N (mg/L)	0.45	0.27	2.3	2.2	0.30	0.28
NO_2^--N (mg/L)	n.m.	0	0	0	n.m.	0
NO_3^--N (mg/L)	n.m.	0.53	0	0	0	0.36
Fe^{2+} (mg/L)	1.2	1.9	28	28	4.5	6.0
Mn^{2+} (mg/L)	0.04	0.9	0.3	0.3	0.2	0.7
SO_4^{2-} (mg/L)	0	16	4.5	5.8	7.3	n.m.
Alkalinity as HCO_3 (mg/L)	245	n.m.	300	300	122	301
Ca^{2+} (mg/L)	60.2	53.3	73.9	71.2	35.6	115
Mg^{2+} (mg/L)	7.2	3.7	4.2	4.1	2.1	13
PO_4^{3-}-P (mg/L)	0.13	0.020	0.28	0.31	0.22	0.21
Si (mg/L)	n.m.	6.5	8.8	8.0	7.0	n.m.

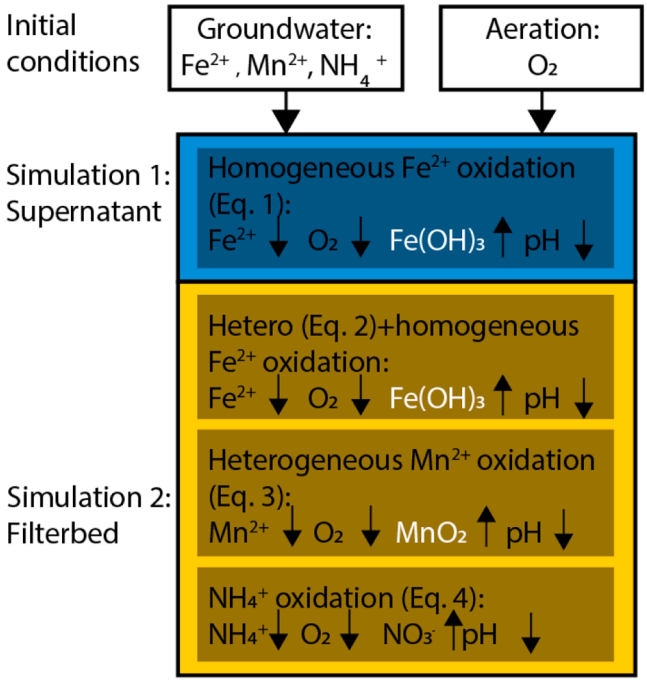

Fig. 2. Simplified conceptual reaction network of simulated coupled processes shown in no particular order of appearance, where arrows pointing up show increasing concentrations and contents and arrows pointing down decreasing concentrations and contents. Solutes and pH are shown in a black font, and solids/precipitates in white.

PHREEQC batch model. The measured water composition after aeration was used as input solution for each filter bed simulation. Unfortunately, the supernatant water composition was not available for RSF-S1, D1, and D2. Therefore, this simulation was not performed for these filters. The presence of both dissolved O_2 and Fe^{2+} initiates homogeneous Fe^{2+} oxidation (Singer and Stumm, 1970; Sung and Morgan, 1980). For simplicity, we assumed that heterogeneous Fe^{2+} oxidation on the precipitated Fe-oxides was neglectable in the supernatant layer, as the Fe-oxide flocs formed were minor and will descend to top of the filter bed. This assumption was also made in the RSF model of Vries et al. (2017). A rate constant of 1.08×10^{-14} mol/L/s was used in these simulations, which corresponds to the obtained homogeneous Fe^{2+} oxidation rate constant at 10 °C obtained by Stuyfzand (2007). We deem this rate constant representable for this study, as the temperatures at all RSFs are comparable ranging from 11–12 °C. The residence time in supernatant (=220–288 seconds), which is also the batch model run time, was estimated by dividing the supernatant level by the flow velocity for each RSF. Model results were written to the output file every two seconds.

2.5. Filter bed simulation

2.5.1. Transport model

The simulated effluent water composition from the supernatant batch model was used as the influent composition of the filter bed simulation. For RSF-S1, D1, and D2 the water composition in the top of the filter bed was used as influent composition as the supernatant composition was not measured for these RSFs. The filter bed was simulated with a 1-dimensional RTM, in which the kinetic processes were simulated as presented in Table 2. The model consisted of 21–26 cells. Cell lengths were determined by dividing the filter bed height (see Table 1) by the number of cells. The duration of each transport time step was calculated as the cell length divided by the flow velocity. We simulated one pore volume during the filter bed simulation using the same number of time steps as model cells. Hydrodynamic dispersion was not simulated to reduce complexity and shorten run-times. Homogeneous Fe^{2+} oxidation was simulated using the same rate equation (equation 1, Table 2) and rate constant (1.08×10^{-14} mol/L/s) as in the supernatant, while homogeneous Mn^{2+} oxidation was not expected to play a role, as the half-life time is in the order of years (Davies and Morgan, 1989; Diem and Stumm, 1984).

2.5.2. Heterogeneous Fe^{2+} and Mn^{2+} oxidation

Heterogeneous Fe^{2+} and Mn^{2+} oxidation likely plays a major role in the filter bed. During heterogeneous oxidation, Fe^{2+} or Mn^{2+} in the influent water is first adsorbed to existing metal-oxide surfaces on the coating of the grains, where it is subsequently oxidized and hydrolysed.

Heterogeneous Fe^{2+} oxidation was simulated based on the rate equation of Tamura (1976) (equation 2, Table 2) with a rate constant of 73 mol/L/s (Tamura, 1976). The Fe^{2+}_{ads} term in the rate equation represents the sites with adsorbed Fe^{2+} on the grain surface. Heterogeneous Mn^{2+} oxidation was simulated using the rate equation of Davies and Morgan (1989), with the proposed rate constant of 2.4×10^{-4} atm^{-1} s^{-1} (equation 3, Table 2). The Mn^{2+}_{ads} term, similarly to Fe^{2+}_{ads}, describes the sites with adsorbed Mn^{2+} on the surface of the grains. Both parameters are depending on the Fe^{2+} and Mn^{2+}-oxide content on the coatings and their adsorption site density. Note that heterogeneous Mn^{2+} oxidation is only occurring on the surface of Mn-oxides and not on Fe-oxides (Gude et al., 2017), while Fe^{2+} oxidation can occur heterogeneously on Mn- and Fe-oxides (Appelo and Postma, 2004).

We used parameter estimation to determine Fe^{2+}_{ads} and Mn^{2+}_{ads} by fitting the simulated dissolved concentrations to the observed concentrations (for more information see Section 2.6). Therefore, surface complexation modelling on the coated grains was not needed, which largely simplified the model and its outcomes and decreased the model runtime. These terms were kept temporally and spatially constant during the model run, as (i) we expect that available sorption sites only negligibly increase during the model run compared to the already available sorption sites on the coating, and (ii) we assumed the terms to be constant over the depth of the filter, as the grains in the rapid sand filter are fully mixed during backwashing resulting in spatially alike coatings.

Biological heterogeneous Fe^{2+} oxidation can also occur in RSFs and is mostly expected when the influent water has a low pH (<7) and is only mildly aerated (Müller et al., 2024). To the best of our knowledge, untangling chemical and biological heterogeneous Fe^{2+} oxidation in rapid sand filters is challenging, and a rate equation for biological heterogeneous Fe^{2+} oxidation does not exist. Therefore, biological heterogeneous Fe^{2+} oxidation was not simulated as an additional process in the model. If biological Fe^{2+} oxidation plays a role in these systems, this will result in an increasing Fe^{2+}_{ads} term for chemical heterogeneous Fe^{2+} oxidation as the rate constant for heterogeneous Fe^{2+} oxidation is kept stable.

2.5.3. Nitrification

In regular RSF conditions, nitrification is a biotic process (Lee et al., 2014; Tatari et al., 2013). There is no standard or regularly used rate equation to simulate this process in reactive transport models. We decided to simulate nitrification using a simple first-order reaction rate equation (equation 4, Table 2), as also reported by Breda et al. (2019), Tatari et al. (2013), and Lopato et al. (2013).

2.6. Parameter optimization using PEST

PEST was used to estimate the unknown parameters (Fe^{2+}_{ads}, Mn^{2+}_{ads}, and k_{NH4}) from the kinetic rate equations for heterogeneous Fe^{2+} and Mn^{2+} oxidation and nitrification. The Gauss-Marquardt-Levenberg method algorithm was used to optimize the fit between the simulated concentrations and the observed concentrations. This process was performed in parallel for Fe^{2+}, Mn^{2+}, and NH_4^+ oxidation process in one PEST run per RSF model. For the dual media filters, we decided to estimate the parameters Fe^{2+}_{ads} and Mn^{2+}_{ads} independently using PEST for both layers.

2.7. Accessibility reactive transport model

The PHREEQC model for RSF-S1 and RSF-D3 plus the corresponding database are available on GitHub: https://github.com/emielkruisdijk/RTM_sandfilter_2024.

Table 2
Kinetic processes simulated in the model, their chemical formulas, and corresponding rate equations.

Eq.	Kinetic process	Chemical formula	Rate equation	Source
1	Homogeneous Fe^{2+} oxidation	$Fe^{2+} + \frac{1}{4}O_2 + 2.5H_2O \leftrightarrow Fe(OH)_3 + 2H^+$	$r_{Fe-homo} = -k\frac{[Fe^{2+}][O_2]}{[H^+]^2}$	Sung and Morgan (1980)
2	Heterogeneous Fe^{2+} oxidation	$Fe^{2+}_{ads} + \frac{1}{4}O_2 + 2.5H_2O \leftrightarrow Fe(OH)_3 + 2H^+$	$r_{Fe-hetero} = -k[Fe^{2+}ads][O_2]$	Tamura (1976)
3	Heterogeneous Mn^{2+} oxidation	$Mn^{2+}_{ads} + \frac{1}{2}O_2 + H_2O \leftrightarrow MnO_2 + 2H^+$	$r_{Mn-hetero} = -k[Mn^{2+}ads]P_{O_2}$	Davies and Morgan (1989)
4	Nitrification	$NH_4^+ + 2O_2 \leftrightarrow NO_3^- + 2H^+ + H_2O$	$r_{NH_4} = -k_{NH4}[NH_4^+]$	-

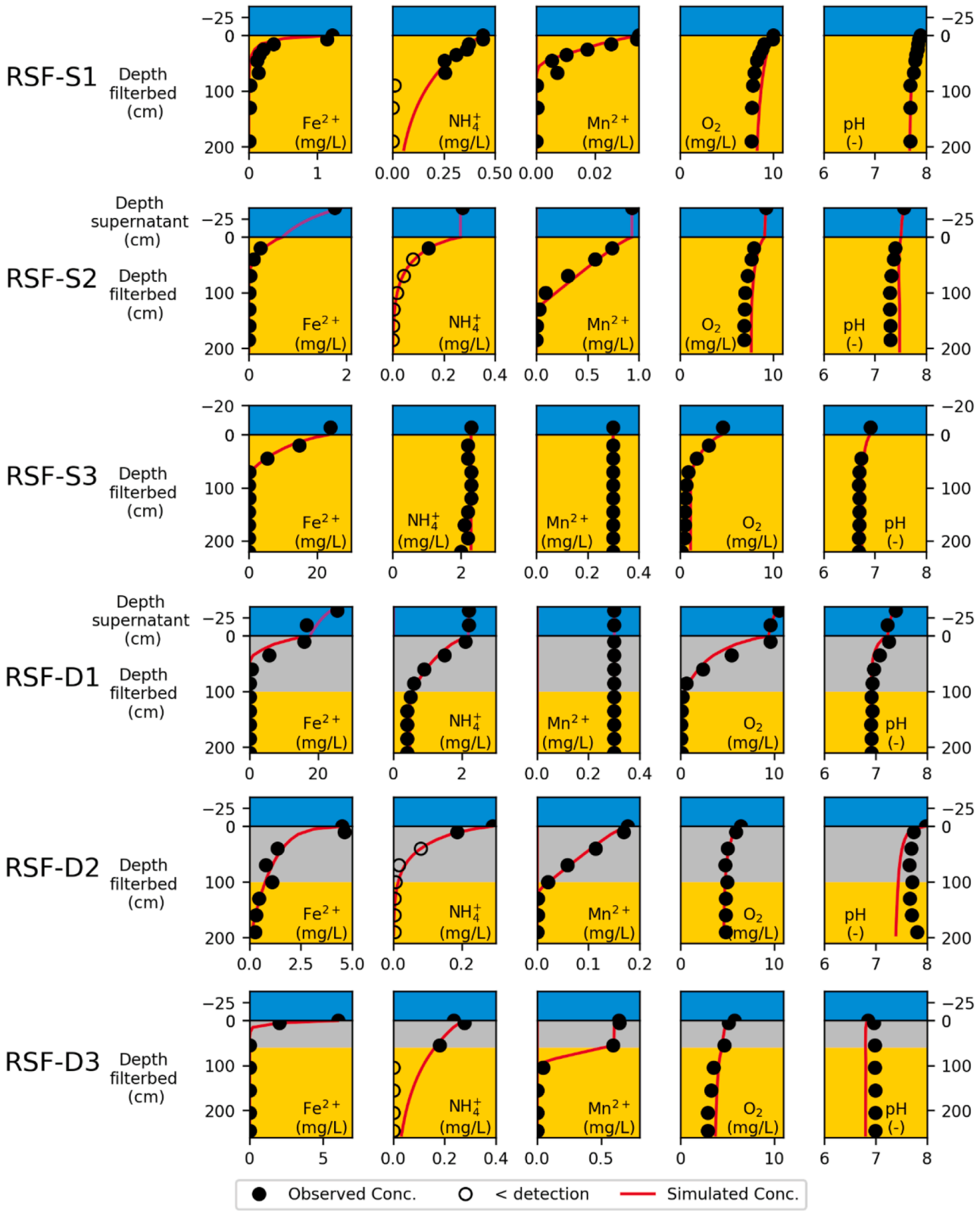

Fig. 3. Observed and simulated solute concentrations and pH with depth in the supernatant and filter bed for six rapid sand filters. The blue, grey, and yellow backgrounds represent supernatant, anthracite, and quartz sands, respectively.

3. Results

3.1. Observed and simulated water quality changes in RSF

Fig. 3 depicts the observed and simulated concentrations over depth in the supernatant and the filter bed for the six RSFs. For all RSFs, a good fit was obtained between observed and simulated Fe^{2+}, Mn^{2+}, NH_4^+, and O_2 concentrations. This shows that there are no other major reductants (like DOC) or oxidants of relevance. Therefore, the oxidation–reduction mass balance seems accurate. Additionally, a good fit (max deviation < 0.2) was obtained between the observed and simulated pH. Only the simulated pH at RSF-D2 was somewhat lower (max deviation ~0.5) than observed, for which no clear explanation can be provided. The model of Vries et al. (2017) consistently underestimated pH and overestimated O_2 concentrations at the five simulated RSFs. They stated that under-estimation of pH could be the result of an over-estimated heterogeneous Fe^{2+} oxidation rate, and that overestimation of the O_2 concentrations could be attributed to the presence of O_2 depleted pockets in the filter or O_2 consumption by biological activity other than nitrifying micro-organisms. The modelling approach presented in the current research does not show these model deficits.

Fe^{2+} was completely removed (> 99%) within the filter bed by all RSFs, however, this was not the case for NH_4^+ and Mn^{2+}. In RSF-S3, all O_2 was consumed by Fe^{2+} oxidation, and, therefore, oxidation of Mn^{2+} and NH_4^+ could not occur. Similarly, Mn^{2+} oxidation did not occur and nitrification was incomplete due to O_2 depletion at RSF-D1. This highlights that Fe^{2+} oxidation occurs before NH_4^+ and Mn^{2+} oxidation, respectively: following the expected sequence in natural systems at circumneutral pH (Appelo and Postma, 2004; Stumm et al., 1996).

3.2. Estimated first order nitrification rate constants

Table 3 shows the estimated first order nitrification rate constants for the six studied RSFs. A rate constant was not calculated for RSF-S3, as nitrification did not appear to happen. The rate constants for nitrification were relatively stable, varying only a factor 3.3, and ranged from 1.3×10^{-3} to 4.3×10^{-3} sec^{-1}. Furthermore, nitrification did not seem to depend on pH (Figure S1), justifying our choice for a nitrification rate equation solely depending on the NH_4^+ concentration. Nitrification occurred similarly on sand grains (RSF-S1, S2) and anthracite grains (RSF-D1, D2, D3). Apparently, the type of grains, nor mineral coating or biofilm age, impacted the oxidation rate. This is noteworthy as often large variations, up to a factor 1000, are observed during biological conversions (Greskowiak et al., 2017; Regnery et al., 2017). These stable rate constants could indicate that nitrification was not substrate (=NH_4^+) and surface limited in the studied RSFs. Based on this hypothesis, we propose that the obtained range of rate constants can be used to forecast the bandwidth of nitrification in RSFs, as long as O_2 is not limiting. Although, this trend should be validated in future research. A better understanding of the relatively stable NH_4^+ oxidation rate constants could be obtained by increasing the number of simulated RSFs.

Table 3
Estimated first order nitrification rate constants in the studied RSFs.

	Single media filters				Dual media filters		
	RSF-S1	RSF-S2	RSF-S3		RSF-D1	RSF-D2	RSF-D3
r_{NH_4} (sec^{-1})	1.3×10^{-3}	2.9×10^{-3}	-*	Top	1.9×10^{-3}	4.3×10^{-3}	2.4×10^{-3}
				Bottom	-*	-*	-*

* Oxidation was not observed, and therefore parameter estimation was not performed

3.3. Estimated heterogeneous Fe^{2+} oxidation rates and pH dependency

For heterogeneous Fe^{2+} oxidation, we assumed the rate constant to be stable and instead estimated Fe^{2+}_{ads} using parameter estimation for all RSFs (Table 4). The rate of heterogeneous Fe^{2+} oxidation increases proportionally to Fe^{2+}_{ads}, making it a proxy for the heterogeneous oxidation rate. In RSF-S1, heterogeneous Fe^{2+} oxidation was not clearly observed and simulation of solely homogeneous Fe^{2+} oxidation gave a good fit. This is likely due to the relatively high pH (7.8) in the influent water, at which homogeneous Fe^{2+} oxidation dominates (van Beek et al., 2012). In the other RSFs, heterogeneous oxidation contributed to Fe^{2+} removal, with Fe^{2+}_{ads} varying from 4.9×10^{-7} mmol/L to 2.7×10^{-4} mmol/L.

Fig. 4 shows the contribution of heterogeneous and homogeneous oxidation to the total Fe^{2+} oxidized for all RSFs. A clear relation with pH is observed: heterogenous Fe^{2+} oxidation dominated at lower pH and homogenous Fe^{2+} oxidation dominated at higher pH, with the turning point at approximately pH=7.7.

Fig. 5 shows the observed homogeneous and heterogeneous Fe^{2+} oxidation rates in the six RSFs. Note that the scales on the x-axis varies approximately two orders of magnitude. The figure clearly shows that homogeneous oxidation contributed substantially to total Fe^{2+} oxidation at RSF-S1, RSF-S2, and RSF-D2 (pH > 7.50), but not at the other RSFs (pH < 7.14). Heterogeneous Fe^{2+} oxidation rates did not seem to depend on dissolved Fe^{2+} concentration, as rates (~1.5×10^{-6} mol/L/s) and pH (~7) in the top layer of the filters of RSF-D1 and RSF-D3 are comparable, while Fe^{2+} concentrations were about 20 mg/L higher in RSF-D1. Maximum Fe^{2+} oxidation rates were found to be 10 to 100-fold higher in the RSFs with the lowest pH (RSF-S3, RSF-D1 and RSF-D3), being the RSFs where heterogeneous oxidation is dominant and very little to no homogeneous oxidation is occurring.

3.4. Estimated heterogeneous Mn^{2+} oxidation rates and relation to grain coating

Table 5 presents the estimated Mn^{2+}_{ads} for the six simulated RSFs. Similar to heterogeneous Fe^{2+} oxidation, the heterogeneous Mn^{2+} oxidation rate increases proportionally to Mn^{2+}_{ads}. In RSF-S3 and D1, Mn^{2+} oxidation was not observed, and rate constants therefore not calculated. In the other RSFs, Mn^{2+}_{ads} was ranging from 1.3×10^{-5} in RSF-D3 to 2.9×10^{-3} in RSF-S2 and seemed not to be depending on pH (S1.). In RSF-D3, heterogeneous Mn^{2+} oxidation increased substantially in the bottom layer (Mn^{2+}_{ads}: 2.2×10^{-3} mmol/L) compared to the top layer (Mn^{2+}_{ads}: 1.3×10^{-5} mmol/L).

Fig. 6 shows microscopic images of the anthracite and sand grains of the dual filter media of RSF-D2 and D3. Within the images, the percentage of Fe- and Mn-coating measured after chemical extraction is shown in pie charts. The grains of RSF-D2 show a mixed coating with a combination of Fe- and Mn-(hydr)oxides. Similarly to the studied single media filters (Figure S2), except for RSF-S3 as there Mn^{2+} oxidation is not occurring. Contrarily, the grains of RSF-D3 show a relatively homogeneous Fe-coating in the anthracite layer, and a relatively

Table 4
Estimated Fe^{2+}_{ads} in the studied RSFs.

	Single media filters				Dual media filters		
	RSF-S1	RSF-S2	RSF-S3		RSF-D1	RSF-D2	RSF-D3
Fe^{2+}_{ads} (mmol/L)	0**	4.9×10^{-7}	2.7×10^{-4}	Top	9.3×10^{-5}	2.9×10^{-6}	9.1×10^{-5}
				Bottom	-*	-*	-*

* Oxidation was not observed, and therefore parameter estimation was not performed

** Solely homogeneous Fe^{2+} oxidation did already fit the observed concentrations well

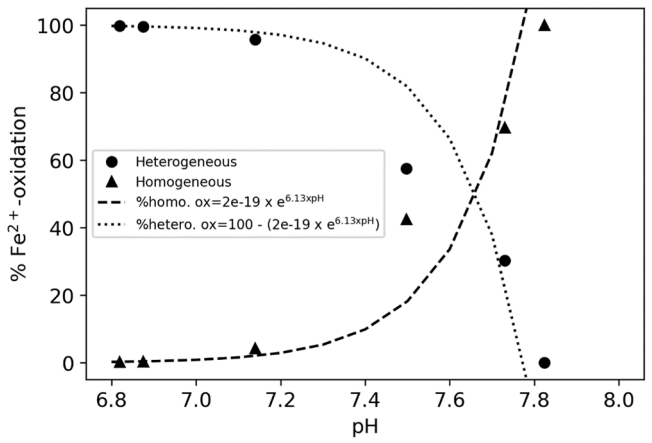

Fig. 4. Contribution of heterogeneous and homogeneous Fe2+ oxidation to the total Fe2+ oxidized determined for each filter bed simulation. An exponential function of pH is shown to estimate the fraction of homogeneous and heterogeneous Fe2+ oxidation. The function was fitted through the percentual contributions of heterogeneous and homogeneous Fe2+ oxidation to the total Fe2+ oxidized.

homogeneous Mn-coating in the sand layer. In the top anthracite layer of RSF-D3, complete Fe^{2+} oxidation is occurring while Mn^{2+} oxidation is almost negligible (Mn^{2+}_{ads}:1.3 × 10^{-5}). Therefore, a relatively homogeneous Fe-coating is formed. In the bottom sand layer the opposite is observed. Mn^{2+} oxidation is ~100 times faster (Mn^{2+}_{ads}: 2.2 × 10^{-3}) than in the top layer, while Fe^{2+} oxidation is not occurring. This results in a relatively homogeneous Mn-coating. This highlights that the Mn^{2+} oxidation rate is likely reflected by the grain coating, as a larger area coated with Mn-(hydr)oxides results in higher adsorbed Mn^{2+}.

4. Discussion

4.1. Fe^{2+} removal accelerates at low pH

Fe^{2+} adsorption generally decreases when the pH is lowered (Appelo et al., 2002; Dixit and Hering, 2006). However, we deduced an increasing Fe^{2+}_{ads} at lower pH, which is directly proportional to more heterogeneous oxidation (Fig. 7**)**. Note, that the model uses a simplified rate equation proposed by Tamura (1976), which was used before in the reactive transport models of Antoniou et al. (2015) and Vries et al. (2017). This rate equation is valid under constant pH and O_2 concentrations, which is not the case in RSFs. It could therefore be attested that the pH-dependent rate equation for heterogeneous Fe^{2+} oxidation proposed by Sung and Morgan (1980) and Tamura et al. (1980) should be used:

$$r_{Fe-hetero} = -k\frac{[Fe^{2+}{}_{ads}][O_2]}{[H^+]} \quad (5)$$

However, this rate equation results in higher rates at higher pH, as both a lower H^+ and a higher adsorbed Fe^{2+} concentration result in increased rates.

Influent water of RSF-S3, D1, and D3 had an approximate pH of 7.0 compared to a pH around 7.75 observed in the other RSFs. Therefore, the H^+ concentrations are roughly 6x higher at pH 7. The observed ~100x higher rates at RSF-S3, D1, and D3, therefore, indicate that Fe^{2+}_{ads} should be 600x higher following equation 5. Assuming that the deposited Fe-oxides have similar site densities in the RSFs, there should be 600x more Fe-oxide coating in RSF-S3, D1, and D3 compared to the other RSFs. The microscope images of the grains (Figure 6 and S2.) do not indicate these substantial variations in Fe-oxide coating. Therefore, the observed higher heterogeneous Fe^{2+} oxidation rates at lower pH likely result from another oxidation pathway. A potential pathway is biological Fe^{2+} oxidation, which can play a major role in RSFs (Müller et al., 2024) and has been reported to become more favourable at lower pH (Kappler et al., 2021). Overall, this highlights the need for more robust and sophisticated rate equations for chemical and biological heterogeneous Fe^{2+} oxidation to increase the predictive capability of reactive transport models. We recommend to increase our

Table 5
Estimated Mn^{2+}_{ads} in the studied RSFs.

	Single media filters				Dual media filters		
	RSF-S1	RSF-S2	RSF-S3		RSF-D1	RSF-D2	RSF-D3
Mn^{2+}_{ads} (mmol/L)	3.5 × 10^{-5}	2.9 × 10^{-3}	-*	Top	-	3.6 × 10^{-4}	1.3 × 10^{-5}
				Bottom	-*	-*	2.2 × 10^{-3}

* Oxidation was not observed, and therefore parameter estimation was not performed

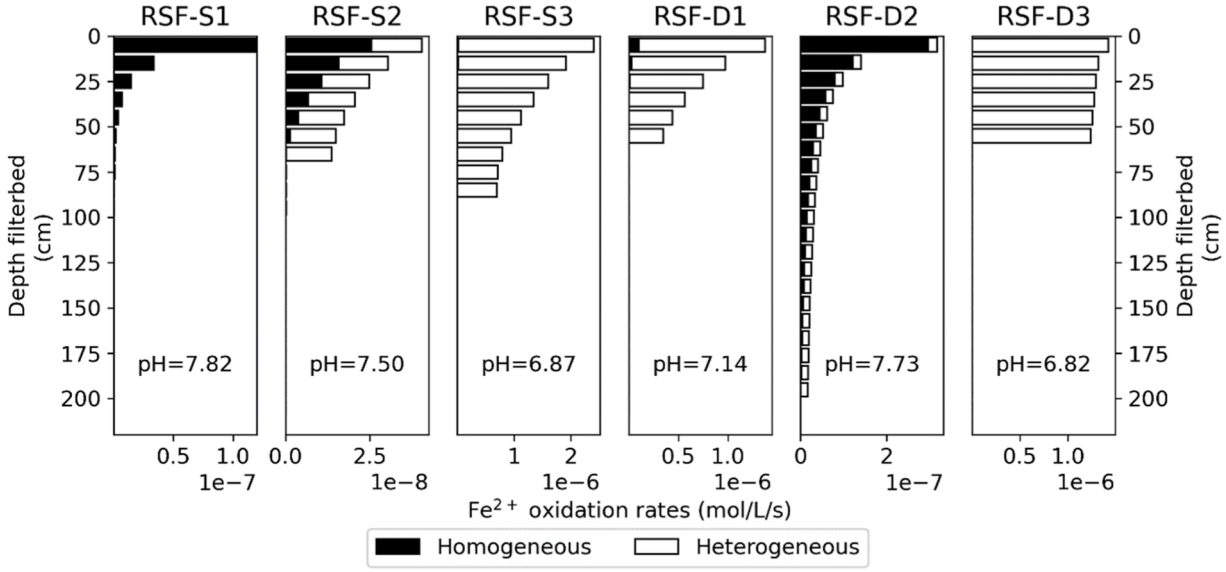

Fig. 5. Homogeneous and heterogeneous Fe^{2+} oxidation rates in the six simulated RSFs and the pH in the top layer of the filter bed.

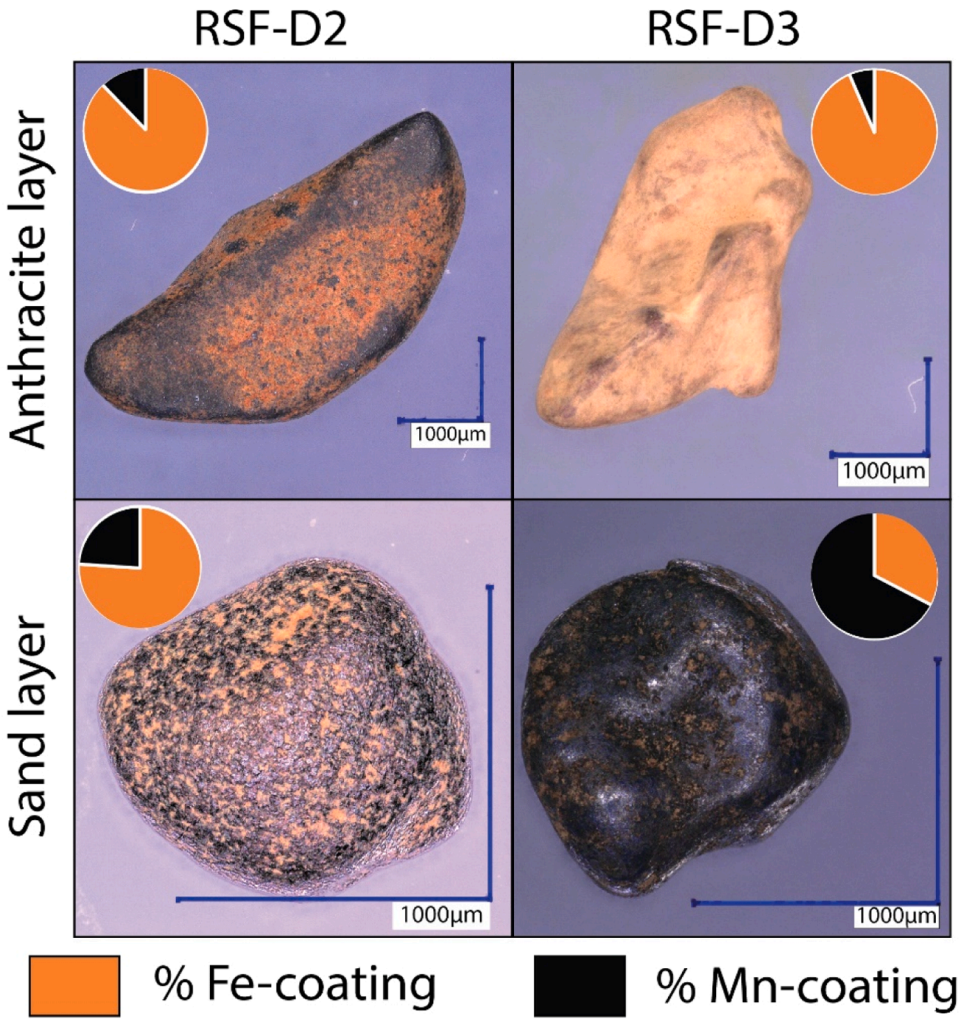

Fig. 6. Microscope images of grains of the anthracite and sand layer of dual media filters RSF-D2 and RSF-D3. The pie chart shows the contribution of iron and manganese in the coating.

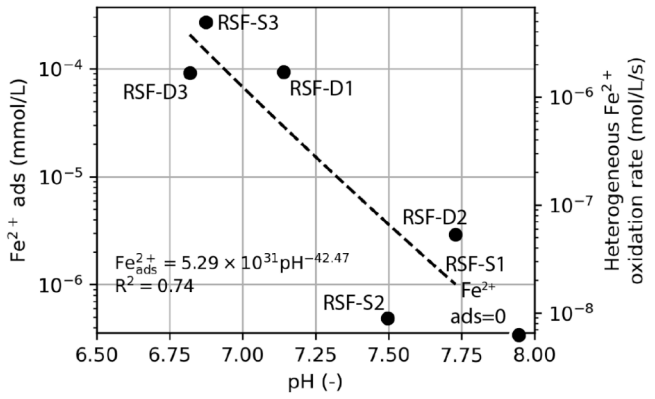

Fig. 7. Relation between the estimated Fe^{2+}_{ads} and the pH in the top layer of the filter bed for the simulated RSFs. The heterogeneous Fe^{2+}rate was added on the right y-axis based on equation 2 with an O_2 concentration of 8 mg/L, as the Fe^{2} adsorbed is proportional to the heterogeneous Fe^{2+}rate. High rates in low pH range suggest biological heterogeneous oxidation instead of chemical heterogeneous oxidation. The equation in the figure shows the relation between Fe^{2+}adsorbed and the pH.

understanding of biological processes in RSFs to potentially distinct biological and chemical oxidation by, for example, studying presences, concentrations, and activities of bacteria available in biofilms.

The higher heterogeneous Fe^{2+} oxidation rates observed at lower pH indicate the potential for operating RSFs under these conditions. A lower pH can be established naturally by limiting aeration and the consequent CO_2 stripping. However, this will also result in lower O_2 concentrations which will negatively influence homogeneous and heterogeneous Fe^{2+} oxidation rates. Compared to operation under higher pH, heterogeneous Fe^{2+} oxidation in the filter will be substantially faster, while the opposite occurs in the supernatant as the lower pH will decrease the rate of homogeneous Fe^{2+} oxidation. As a side effect, this will cause growth of Fe-oxide coatings on the grains in the filter. Müller et al. (2007) showed that operating a RSF at lower pH and, consequently, more heterogeneous Fe^{2+} oxidation caused (i) less clogging allowing for a lower backwash frequency and (ii) potential for operation under higher flow rates. The RTM can help to assess the trade-offs between these processes on RSF operation at lower pH by simulating homogeneous Fe^{2+} oxidation following the rate equation stated in Table 2 and heterogeneous Fe^{2+} oxidation using the trendline in Fig. 7.

4.2. Reactive surface controls manganese(II)-oxidation

Fig. 8 shows the relation between the dissolved Fe^{2+}/Mn^{2+} fraction in the top layer of the filter bed and the derived Mn^{2+}_{ads}. Dissolved $Fe^{2+}/$

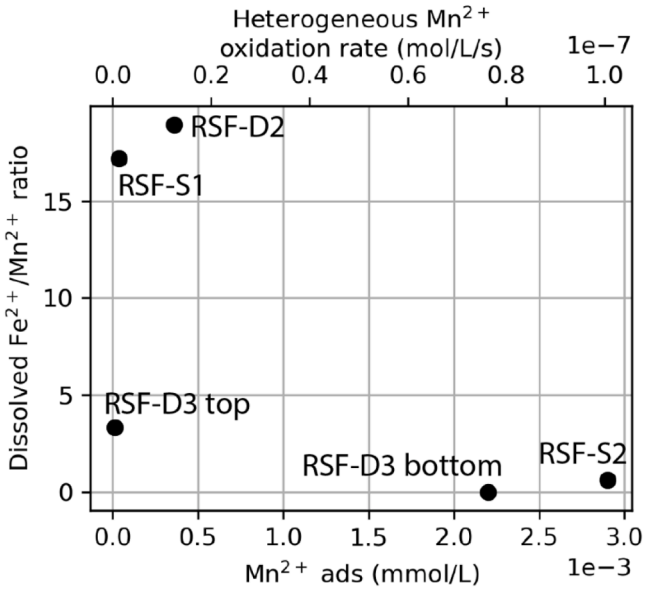

Fig. 8. Fe^{2+} to Mn^{2+} ratio in supernatant versus the Mn^{2+}_{ads} in mmol/L on bottom x-axis. The heterogeneous Mn^{2+} oxidation rate was added on the top x-axis based on equation 3 with an O_2 concentration of 8 mg/L and a temperature of 10 °C, as the Mn^{2+}_{ads} is proportional to the heterogeneous Mn^{2+} oxidation rate.

Mn^{2+} ratios seem to be inversely proportional to Mn^{2+}_{ads}, which indicates that Mn^{2+} oxidation is surface limited as adsorbed Mn^{2+} is lower when Fe^{2+}/Mn^{2+} ratios are higher. This shows the importance of Mn-coated surface for heterogeneous oxidation. This relation is further highlighted in RSF-D3, where adsorbed Mn^{2+} is almost a factor 100 higher in the bottom sand layer as compared to the top anthracite layer, when the dissolved Fe^{2+}/Mn^{2+} ratio drops to zero (Table 5). Consequently, Fig. 6 shows that the top layer contains mostly Fe-coated grains and the bottom layer Mn-coated grains, which clearly shows the effect of a high (RSF-D3 top anthracite layer) compared to a low Fe^{2+}/Mn^{2+} ratio (RSF-D3 bottom sand layer).

Single media filters have a mixed Fe- and Mn-coating, which lowers the Mn^{2+} oxidation rates due to the limited Mn-(hydr)oxide surface available for Mn^{2+} sorption prior to heterogeneous oxidation. We assume that this metal surface availability influences Fe^{2+} oxidation rates to a lesser extent, as this is likely compensated by Fe^{2+} oxidation coupled to reduction of Mn-oxides (Postma, 1985; Postma and Appelo, 2000). Furthermore, to our knowledge, a mixed Fe- and Mn-coating does not negatively affect growth of potential Fe-oxidizing bacteria.

4.3. Separating Fe and Mn oxide layers in sand filters

This study has shown that sequential Fe^{2+} and Mn^{2+} removal and consequent uniform metal coatings on the sand grains, eliminates surface limitation of the oxidation reactions. This is especially beneficial for the treatment of Mn^{2+} from groundwater with relatively high Fe^{2+} and low Mn^{2+} concentrations, where surface limitation is substantial in single media filters. Another potential advantage is that extracted grains have more value for re-use due to their more homogeneous Fe- or Mn-coating (e.g., Chardon et al., 2022; Gupta et al., 2005). Sequential Fe^{2+} and Mn^{2+} oxidation is occurring when the following conditions in the RSF are met: (i) influent water contains Fe^{2+} and Mn^{2+}, (ii) Fe^{2+} oxidation occurs mainly in the top anthracite layer, and Mn^{2+} oxidation in the bottom sand layer, and (iii) both layers should not be mixed during backwashing of the RSF.

The current study focussed on RSFs where first aeration and then filtration occurred. These type of RSFs are commonly found in Western Europe, for example in Denmark (Hedegaard and Albrechtsen, 2014) and Germany (Meffe et al., 2010), but also in non-European countries like Bangladesh (Uddin et al., 2019) and Argentina (Araya-Obando et al., 2022). Note that there are also RSFs where chemical oxidants replace aeration, or where reactive filter material (e.g., TiO_2) is used instead of anthracite/sand. These operational differences can effect the sequence of oxidation, and are, therefore, not part of this research.

The reactive transport model presented in this study can be used to predict the design requirements to achieve sequential removal in dual bed filters. To avoid the formation of mixed mineral coatings, Fe^{2+} oxidation should mainly occur in the top layer (of anthracite or pumice), and Mn^{2+} oxidation in the bottom sand layer. In other words, the depth of the anthracite layer, or alternative low density top layer (e.g., pumice), should be chosen precisely upon complete Fe^{2+} oxidation, but prior to the onset of Mn^{2+} oxidation (Fig. 9A). The position of the tipping point is controlled by the concentrations of Fe^{2+} in the influent water, the oxidation rate, and the flow rate. If Fe^{2+} is oxidized faster than the residence time in the top layer, Mn^{2+} will also oxidize in this top layer and a mixed Fe- and Mn-coating will be formed (Fig. 9B). At the same time, if Fe^{2+} oxidation is too slow, a part of the Fe^{2+} oxidation will take place in the bottom layer, and therefore a mixed Fe- and Mn-coating will be formed at the grains in the bottom layer (Fig. 9C).

For the design of new RSFs, the depth of complete Fe^{2+} oxidation can be approximated by, (i) estimating the heterogeneous Fe^{2+} oxidation rate based on the influent water pH and the equation shown in Fig. 7, and (ii) deducing this depth after simulating heterogeneous Fe^{2+} oxidation using the RTM. This method can give an useful first estimate of the complete Fe^{2+} oxidation depth. However, note that the obtained depth of complete Fe^{2+} oxidation comes with some uncertainty, as the trendline in Fig. 7 is only based on six RSFs and the fit is not perfect (R^2=0.74). Therefore, we recommend to validate this observed trend in future research and to make it more reliable and accurate by increasing the number of simulated RSFs.

The depth of complete Fe^{2+} oxidation can be monitored by periodical sampling and analysing the water for Fe^{2+} and Mn^{2+} exactly at the depth of the division of the two layers and compare this to the influent water composition. When complete Fe^{2+} oxidation is not observed at the intersection depth of both layers during operation, the RTM can be used to determine how this can be solved. First, the kinetic oxidation parameters (r_{NH_4}, Fe^{2+}_{ads}, and Mn^{2+}_{ads}) should be obtained using parameter estimation. Second, model scenarios should be performed with various flow velocities and/or filter bed heights, to optimize the depth of complete Fe^{2+} oxidation. Based on the outcomes, complete Fe^{2+} oxidation can be established at the right depth by increasing or decreasing the flow velocity or adding or removing anthracite to adapt the thickness of the top layer.

Furthermore, the developed RTM can be used to simulate the effects of operational changes in RSF operation on Fe^{2+}, Mn^{2+}, and NH_4^+ removal. For example, (i) to study the effects of seasonal variations in water demand, which can be examined by changing the flow of the influent groundwater, or (ii) to analyse the impact of influent water composition changes, which often occurs in practice as RSF are regularly treating water from alternating (mixtures of) groundwater wells.

5. Conclusion

In this study, we demonstrated through reactive transport modelling of full-scale rapid sand filters (RSFs) that controlling Fe and Mn mineral coatings on filter grains is crucial for achieving optimal removal of both metals. Fe^{2+} and Mn^{2+} oxidation occurred mainly simultaneously in the studied RSFs, rather than sequentially as expected based on Gibbs free energy calculations. This is caused by full mixing of the grains during backwashing, which initiates heterogeneous Mn^{2+} oxidation on the Mn-coated grains that end up in the upper layer of the filter. The resulting mixed Fe/Mn coatings limit Mn^{2+} removal by heterogeneous oxidation due to the limitedly available Mn-oxide surfaces on the grains. This rate limitation can be prevented by designing filters with two separate layers of specific thickness where Fe^{2+} and Mn^{2+} oxidation occurs sequentially

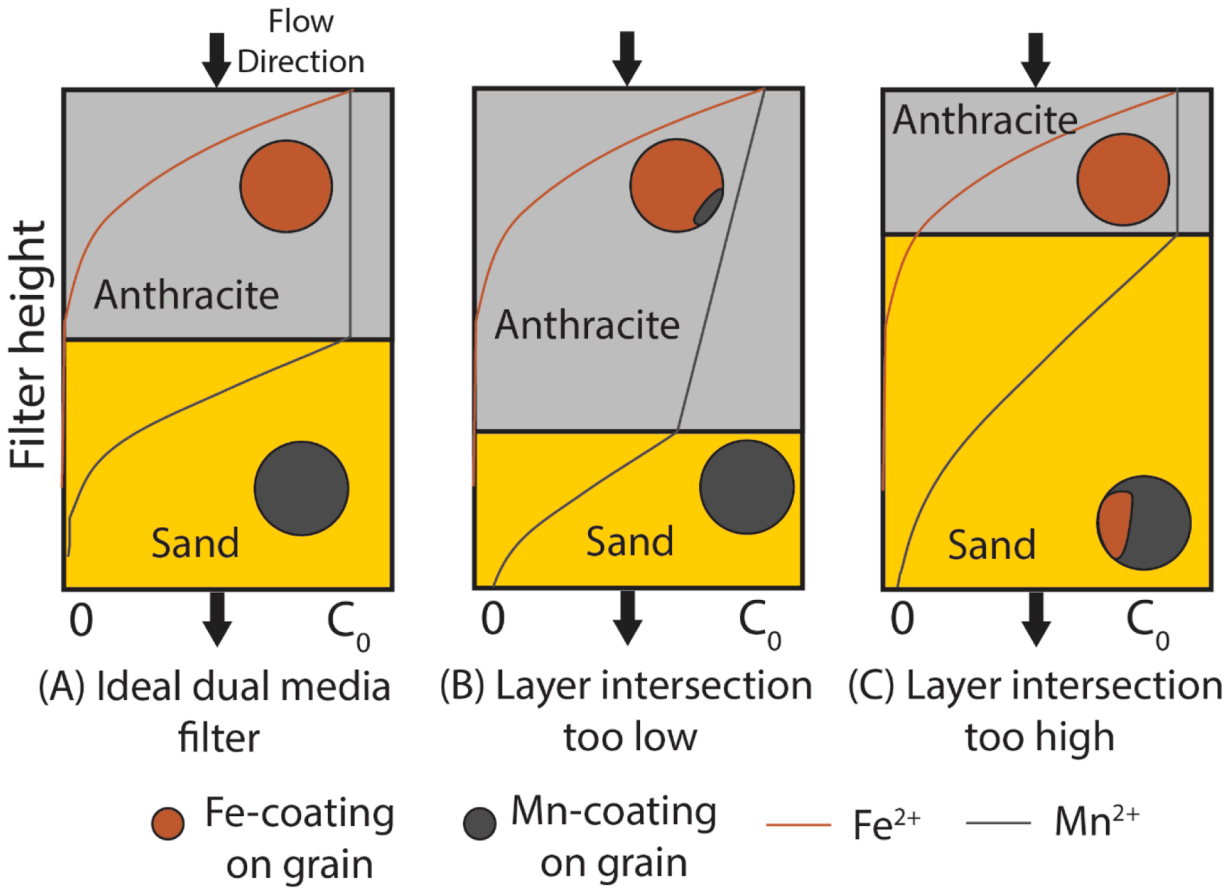

Fig. 9. Design considerations for a sequential Fe^{2+} and Mn^{2+} oxidizing rapid sand filter.

resulting in uniform mineral coatings. To design a filter with spatial separation of processes, complete Fe^{2+} oxidation should occur in the top layer. Using the developed RTM, we can approximate the intersection depth of the top anthracite and bottom sand layer.

CRediT authorship contribution statement

Emiel Kruisdijk: Writing – review & editing, Writing – original draft, Visualization, Software, Methodology, Formal analysis, Data curation, Conceptualization. **Boris M. van Breukelen:** Writing – review & editing, Validation, Supervision, Methodology, Conceptualization. **Doris van Halem:** Writing – review & editing, Visualization, Validation, Supervision, Project administration, Methodology, Funding acquisition, Data curation, Conceptualization.

Declaration of competing interest

The authors declare that they have no known competing financial interests or personal relationships that could have appeared to influence the work reported in this paper.

Data availability

Data will be made available on request.

Acknowledgements

The authors would like to thank Frank Schoonenberg and Jink Gude for making data available and the thorough discussions. This work was financed by the Netherlands Organisation for Scientific Research (NWO): project 17830 and 18369.

Supplementary materials

Supplementary material associated with this article can be found, in the online version, at doi:10.1016/j.watres.2024.122517.

References

Antoniou, E.A., Stuyfzand, P.J., van Breukelen, B.M., 2013. Reactive transport modeling of an aquifer storage and recovery (ASR) pilot to assess long-term water quality improvements and potential solutions. Appl. Geochem. 35, 173–186.
Antoniou, E.A., van Breukelen, B.M., Stuyfzand, P.J., 2015. Optimizing aquifer storage and recovery performance through reactive transport modeling. Appl. Geochem. 61, 29–40.
Appelo, C.A.J., Postma, D., 2004. Geochemistry, Groundwater and Pollution. CRC press.
Appelo, C.A.J., Van der Weiden, M.J.J., Tournassat, C., Charlet, L., 2002. Surface complexation of ferrous iron and carbonate on ferrihydrite and the mobilization of arsenic. Environ. Sci. Technol. 36, 3096–3103.
Araya-Obando, J.A., Pacini, V., Fernández, R.G., Romero-Esquivel, L.G., 2022. Long-term monitoring of Mn and Fe removal in biofilters from a converted plant. Water Supply 22, 6059–6069.
Beckingham, L.E., Mitnick, E.H., Steefel, C.I., Zhang, S., Voltolini, M., Swift, A.M., Yang, L., Cole, D.R., Sheets, J.M., Ajo-Franklin, J.B., DePaolo, D.J., Mito, S., Xue, Z. Q., 2016. Evaluation of mineral reactive surface area estimates for prediction of reactivity of a multi-mineral sediment. Geochim. Cosmochim. Acta 188, 310–329.
Breda, I.L., Ramsay, L., Søborg, D.A., Dimitrova, R., Roslev, P., 2019. Manganese removal processes at 10 groundwater fed full-scale drinking water treatment plants. Water Qual. Res. J. 54, 326–337.
Chardon, W.J., Groenenberg, J.E., Vink, J.P.M., Voegelin, A., Koopmans, G.F., 2022. Use of iron-coated sand for removing soluble phosphorus from drainage water. Sci. Total Environ. 815, 152738.
Connor, R., 2015. The United Nations World Water Development Report 2015: Water for a Sustainable World. UNESCO publishing.
Corbera-Rubio, F., Laureni, M., Koudijs, N., Müller, S., van Alen, T., Schoonenberg, F., Lücker, S., Pabst, M., van Loosdrecht, M.C.M., van Halem, D., 2023. Meta-omics profiling of full-scale groundwater rapid sand filters explains stratification of iron, ammonium and manganese removals. Water. Res. 233, 119805.

Davies, S.H.R., Morgan, J.J., 1989. Manganese(II) oxidation kinetics on metal oxide surfaces. J. Colloid. Interface Sci. 129, 63–77.
Diem, D., Stumm, W., 1984. Is dissolved Mn2+ being oxidized by O2 in absence of Mn-bacteria or surface catalysts? Geochim. Cosmochim. Acta 48, 1571–1573.
Dixit, S., Hering, J.G., 2006. Sorption of Fe(II) and As(III) on goethite in single- and dual-sorbate systems. Chem. Geol. 228, 6–15.
Doherty, J., 1994. PEST: Model Independent Parameter Estimation. Brisbane, Australia.
Freitas, B.L.S., Terin, U.C., Fava, N.M.N., Maciel, P.M.F., Garcia, L.A.T., Medeiros, R.C., Oliveira, M., Fernandez-Ibañez, P., Byrne, J.A., Sabogal-Paz, L.P., 2022. A critical overview of household slow sand filters for water treatment. Water. Res. 208, 117870.
Greskowiak, J., Hamann, E., Burke, V., Massmann, G., 2017. The uncertainty of biodegradation rate constants of emerging organic compounds in soil and groundwater – a compilation of literature values for 82 substances. Water. Res. 126, 122–133.
Gude, J.C.J., Rietveld, L.C., van Halem, D., 2016. Fate of low arsenic concentrations during full-scale aeration and rapid filtration. Water. Res. 88, 566–574.
Gude, J.C.J., Rietveld, L.C., van Halem, D., 2017. As(III) oxidation by MnO2 during groundwater treatment. Water. Res. 111, 41–51.
Gupta, V.K., Saini, V.K., Jain, N., 2005. Adsorption of As(III) from aqueous solutions by iron oxide-coated sand. J. Colloid. Interface Sci. 288, 55–60.
Haukelidsaeter, S., Boersma, A.S., Kirwan, L., Corbetta, A., Gorres, I.D., Lenstra, W.K., Schoonenberg, F.K., Borger, K., Vos, L., van der Wielen, P.W.J.J., van Kessel, M.A.H. J., Lücker, S., Slomp, C.P., 2023. Influence of filter age on Fe, Mn and NH4+ removal in dual media rapid sand filters used for drinking water production. Water. Res. 242, 120184.
Hedegaard, M.J., Albrechtsen, H.-J., 2014. Microbial pesticide removal in rapid sand filters for drinking water treatment – Potential and kinetics. Water. Res. 48, 71–81.
Kappler, A., Bryce, C., Mansor, M., Lueder, U., Byrne, J.M., Swanner, E.D., 2021. An evolving view on biogeochemical cycling of iron. Nature Rev. Microbiol. 19, 360–374.
Kruisdijk, E., van Breukelen, B.M., 2021. Reactive transport modelling of push-pull tests: a versatile approach to quantify aquifer reactivity. Appl. Geochem. 131, 104998.
Lee, C.O., Boe-Hansen, R., Musovic, S., Smets, B., Albrechtsen, H.-J., Binning, P., 2014. Effects of dynamic operating conditions on nitrification in biological rapid sand filters for drinking water treatment. Water. Res. 64, 226–236.
Lopato, L., Röttgers, N., Binning, P.J., Arvin, E., 2013. Heterogeneous nitrification in a full-scale rapid sand filter treating groundwater. J. Environ. Eng. 139, 375–384.
Meffe, R., Kohfahl, C., Holzbecher, E., Massmann, G., Richter, D., Dünnbier, U., Pekdeger, A., 2010. Modelling the removal of p-TSA (para-toluenesulfonamide) during rapid sand filtration used for drinking water treatment. Water. Res. 44, 205–213.
Müller, K., Magesan, G.N., Bolan, N.S., 2007. A critical review of the influence of effluent irrigation on the fate of pesticides in soil. Agric. Ecosyst. Environ. 120, 93–116.
Müller, S., Corbera-Rubio, F., Schoonenberg-Kegel, F., Laureni, M., Loosdrecht, M.C.M. v., Halem, D.v., 2024. Shifting to biology promotes highly efficient iron removal in groundwater filters. bioRxiv. 2024.2002.2014.580244.
Parkhurst, D.L., Appelo, C.A.J., 2013. Description of input and examples for PHREEQC version 3: a computer program for speciation, batch-reaction, one-dimensional transport, and inverse geochemical calculations 519.
Postma, D., 1985. Concentration of Mn and separation from Fe in sediments—I. Kinetics and stoichiometry of the reaction between birnessite and dissolved Fe(II) at 10°C. Geochim. Cosmochim. Acta 49, 1023–1033.
Postma, D., Appelo, C.A.J., 2000. Reduction of Mn-oxides by ferrous iron in a flow system: column experiment and reactive transport modeling. Geochim. Cosmochim. Acta 64, 1237–1247.
Rahman, M.M., Bakker, M., Patty, C.H.L., Hassan, Z., Roling, W.F.M., Ahmed, K.M., van Breukelen, B.M., 2015. Reactive transport modeling of subsurface arsenic removal systems in rural Bangladesh. Sci. Total Environ. 537, 277–293.
Regnery, J., Gerba, C.P., Dickenson, E.R.V., Drewes, J.E., 2017. The importance of key attenuation factors for microbial and chemical contaminants during managed aquifer recharge: a review. Crit. Rev. Environ. Sci. Technol. 47, 1409–1452.
Siade, A.J., Bostick, B.C., Cirpka, O.A., Prommer, H., 2021. Unraveling biogeochemical complexity through better integration of experiments and modeling. Environ. Sci.: Process. Impacts 23, 1825–1833.
Singer, P.C., Stumm, W., 1970. Acidic mine drainage: the rate-determining step. Science (1979) 167, 1121–1123.
Steefel, C.I., DePaolo, D.J., Lichtner, P.C., 2005. Reactive transport modeling: an essential tool and a new research approach for the Earth sciences. Earth. Planet. Sci. Lett. 240, 539–558.
Stumm, W., Morgan, J.J., Drever, J.I., 1996. Aquatic chemistry. J. Environ. Qual. 25, 1162.
Stuyfzand, P., 2007. Towards a more effective diagnosis, therapy and prevention of chemical well and drain clogging. H2O 44–47, 2007.
Sung, W., Morgan, J.J., 1980. Kinetics and products of ferrous iron oxygenation in aqueous systems. Environ. Sci. Technol. 14, 561–568.
Tamura, H., Katsumi, G., Nagayama, M., 1976. The effect of ferric hydroxide on the oxygenation of ferrous ions in neutral solutions. Corros. Sci. 16, 197–207.
Tamura, H., Kawamura, S., Hagayama, M., 1980. Acceleration of the oxidation of Fe2+ ions by Fe(III)-oxyhydroxides. Corros. Sci. 20, 963–971.
Tatari, K., Smets, B.F., Albrechtsen, H.J., 2013. A novel bench-scale column assay to investigate site-specific nitrification biokinetics in biological rapid sand filters. Water. Res. 47, 6380–6387.
Tebo, B.M., Johnson, H.A., McCarthy, J.K., Templeton, A.S., 2005. Geomicrobiology of manganese(II) oxidation. Trends. Microbiol. 13, 421–428.
Tekerlekopoulou, A.G., Pavlou, S., Vayenas, D.V., 2013. Removal of ammonium, iron and manganese from potable water in biofiltration units: a review. J. Chem. Technol. Biotechnol. 88, 751–773.
Uddin, M.M., Kurisu, F., Kasuga, I., Furumai, H., Islam, S.M.A., 2019. Potential of biological arsenite oxidation in sand filtration units at arsenic–iron removal plants (AIRPs) in Bangladesh. Appl. Water. Sci. 9, 48.
van Beek, C.G.E.M., Hiemstra, T., Hofs, B., Nederlof, M.M., van Paassen, J.A.M., Reijnen, G.K., 2012. Homogeneous, heterogeneous and biological oxidation of iron (II) in rapid sand filtration. J. Water Suppl.: Res. Technol.-Aqua 61, 1–13.
van Kessel, M.A.H.J., Speth, D.R., Albertsen, M., Nielsen, P.H., Op den Camp, H.J.M., Kartal, B., Jetten, M.S.M., Lücker, S., 2015. Complete nitrification by a single microorganism. Nature 528, 555–559.
Vries, D., Bertelkamp, C., Schoonenberg Kegel, F., Hofs, B., Dusseldorp, J., Bruins, J.H., de Vet, W., van den Akker, B., 2017. Iron and manganese removal: recent advances in modelling treatment efficiency by rapid sand filtration. Water. Res. 109, 35–45.
Zouboulis, A., Traskas, G., Samaras, P., 2007. Comparison of single and dual media filtration in a full-scale drinking water treatment plant. Desalination. 213, 334–342.